Direct Observation of Weak Hydrogen Bonds in Microsolvated Phenol: Infrared Spectroscopy of OH Stretching Vibrations of Phenol−CO and $-CO_2$ in S_0 and D_0

Asuka Fujii,* Takayuki Ebata, and Naohiko Mikami*

Department of Chemistry, Graduate School of Science, Tohoku University, Sendai 980-8578, Japan

Received: May 21, 2002; In Final Form: August 7, 2002

Infrared spectroscopy was applied to phenol−CO and phenol−CO_2 clusters in a molecular beam, and the OH stretching vibrations of these clusters were observed both in their neutral (S_0) and in their cationic (D_0) ground states. Their OH frequency in S_0 shows a small but definite low-frequency shift, indicating that the phenol moiety acts as a proton donor in their hydrogen-bonded structures. The magnitude of the frequency shifts well correlates with proton affinities of the proton-accepting CO and CO_2 molecules. The OH stretching vibrations in D_0 showed a substantial low-frequency shift, representing that the hydrogen-bond strength is remarkably enhanced upon ionization. Density functional theoretical calculations of the cluster structures were carried out to support discussion.

I. Introduction

Molecular clusters of phenol with various proton acceptors have extensively been studied for the microscopic information on hydrogen bonds.[1−5] Recently, Müller-Dethlefs and coworkers reported peculiar characters of phenol−N_2 and phenol−CO.[6−10] They observed the S_1-S_0 electronic, zero kinetic energy (ZEKE) photoelectron, and mass-analyzed threshold ionization (MATI) spectra of these clusters. On the basis of these spectroscopic results and ab initio calculations, it was concluded that both of these clusters have an in-plane structure, in which the N-end or C-end of the solvent molecule is bound to the hydroxyl group of the phenol site, both in the neutral (S_0) and in the cationic (D_0) ground states. Such a cluster structure means that in these clusters the σ-hydrogen bonding is predominant over the van der Waals interactions, which often lead to an on-top structure as seen in benzene−N_2.[11] The intermolecular binding energies in S_0 are estimated to be only 435 ± 20 and 659 ± 20 cm^{-1} for phenol−N_2 and −CO, respectively,[6,7] and such a small binding energy may not be good enough to verify the σ-hydrogen-bonded structure. These values are actually close to a typical van der Waals bond energy ($\sim$300 cm^{-1}) in many aromatic molecular clusters rather than typical σ-hydrogen-bond energy ($\sim$2000 cm^{-1}).[12,13] On the other hand, the hydrogen-bond energy in D_0 is estimated to be 1640 ± 10 and 2425 ± 10 cm^{-1} for phenol−N_2 and −CO, respectively, indicating a significant enhancement of the hydrogen-bond strength upon ionization.[6,7]

To characterize such a peculiar feature of these hydrogen bonds, spectroscopic investigation of the OH stretching vibrations would give us the most direct information. In our previous paper, we applied infrared (IR) spectroscopy to phenol−N_2 in S_0 and D_0.[14] An extremely small but distinct OH frequency shift was observed in S_0, representing a direct evidence for the extraordinary weak hydrogen-bond formation in its neutral ground state. A much larger OH frequency shift was found in the cation produced by resonance-enhanced multiphoton ionization (REMPI) of the neutral cluster, supporting the drastic enhancement of the hydrogen-bond strength upon ionization. Solcà and Dopfer also applied IR spectroscopy to the cluster cation prepared by a pick-up-type ion source, in which electron impact ionization of bare phenol is followed by three-body collisions.[15,16] Such an ion source predominantly produces cluster cations in the most stable structure. The IR spectrum measured by Solcà and Dopfer was essentially identical with that of the REMPI-produced cluster ion, and it was confirmed that the hydrogen-bonded structure is the global minimum in the potential surface of (phenol−N_2)$^+$.

In the present paper, as an extension of our previous work, we report IR spectroscopy of the phenol−CO and $-CO_2$ clusters in both S_0 and D_0. On the basis of OH frequency shifts upon the cluster formation, the nature of the intermolecular interactions in these clusters is examined.

II. Experiment

The infrared−ultraviolet (IR−UV) double-resonance technique was used for IR spectroscopy in S_0, while IR spectra in D_0 were obtained by using infrared photodissociation (IRPD) spectroscopy. Because both techniques have been described elsewhere in detail,[3,14] here we give only a brief description of the methods.

A. IR−UV Double-Resonance Spectroscopy in S_0. A pulsed UV laser of which wavelength is fixed at the origin band of the S_1-S_0 transition of the cluster is introduced, and the REMPI signal is observed as a measure of the ground-state population. Prior to the UV laser, an IR laser pulse is introduced, and its wavelength is scanned. When the IR wavelength is resonant on a vibrational transition of the cluster, the IR absorption induces a reduction of the ground-state population, and it is detected as a decrease of the REMPI signal intensity.

B. IRPD Spectroscopy in D_0. The cluster cation is produced by two-color REMPI of the corresponding neutral cluster to suppress the internal energy of the cluster cations. The first UV laser excites a neutral cluster to the vibrational ground level of S_1, and the second UV laser ionizes it. The second UV laser wavelength is fixed at 330 and 315 nm for the ionization of phenol−CO and $-CO_2$, respectively. After a delay time of 50 ns, the IR laser pulse is introduced. When the IR wavelength is resonant on a vibrational transition of the cluster ion, the vibrational excitation causes vibrational predissociation of the

10.1021/jp0212601 CCC: $22.00
Published on Web 09/27/2002

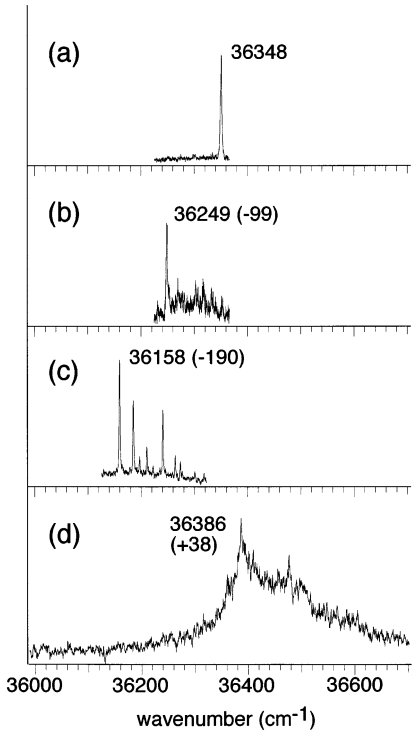

Figure 1. Resonance-enhanced multiphoton ionization (REMPI) spectra of (a) bare phenol, (b) phenol−N_2, (c) phenol−CO, and (d) phenol−CO_2 in the origin band region of the S_1-S_0 electronic transition. The parent ion intensity is measured in each spectrum.

cluster ion, leading to a depletion of the cluster ion intensity. Thus, by scanning the IR wavelength while monitoring the cluster ion intensity, we obtain the IR spectrum of the cluster ion as the depletion spectrum.

The sample of phenol was kept at room temperature, and its vapor was seeded in the He/Ar/CO (or CO_2) mixture carrier gas of 3 atm stagnation pressure. The concentration of the solvent molecule (CO or CO_2) in the mixture gas was 10%. The pulsed jet expansion of the gaseous mixture was skimmed by a skimmer of 2 mm diameter, and the resultant molecular beam was introduced into the interaction region. A time-of-flight mass spectrometer was used for the mass separation of ions.

III. Results and Discussion

A. S_1-S_0 Electronic Spectra. Figure 1 shows the mass-selected REMPI spectra of (a) bare phenol, (b) phenol−N_2, (c) phenol−CO, and (d) phenol−CO_2 in their S_1-S_0 origin (0−0) band region. Each spectrum was obtained by monitoring the parent (cluster) cation. The origin bands of phenol−N_2 and −CO appear at 36 249 and 36 158 cm^{-1}, respectively, and they show the low-frequency shifts of −99 and −190 cm^{-1} from that of bare phenol. Some intermolecular vibration bands associated with the origin band are also seen in the spectra. Detailed analysis of these intermolecular vibration bands has already been carried out in the first report of these electronic transitions by Haines et al.[6,7]

On the other hand, the electronic spectrum of phenol−CO_2, which is reported for the first time in this paper, is significantly different from those of the other clusters. A rather sharp band being overlaid by broad background absorption is seen at 36 386 cm^{-1}, which is on the *high*-frequency side of +38 cm^{-1} from the origin band of bare phenol. This band is assigned to the origin band of phenol−CO_2 because no band appears in the lower-frequency region. The broad background of the spectrum is attributed to higher clusters. Though the intensity of the 1:1 cluster cation was detected for the spectrum, dissociation following ionization prevented us from eliminating the contribution of higher clusters.

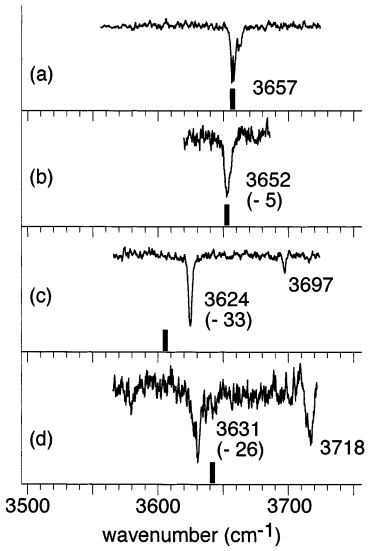

Figure 2. OH stretching vibrational region of infrared (IR) spectra of (a) bare phenol, (b) phenol−N_2, (c) phenol−CO, and (d) phenol−CO_2 in the neutral ground state (S_0). The IR−UV double-resonance spectroscopic technique is utilized to measure the spectra. Values in the parentheses are the shifts from the OH vibrational frequency of bare phenol. Bar graphs under the observed spectra show the calculated OH stretching vibrational frequencies based on the energy-optimized structures at the B3LYP/6-31G(d,p) level (see text).

B. Infrared Spectra in S_0. The OH stretching vibrational region of the IR spectra of (a) bare phenol, (b) phenol−N_2, (c) phenol−CO, and (d) phenol−CO_2 in S_0 is shown in Figure 2. The spectra of bare phenol and phenol−N_2 are reproduced from our previous paper,[14] so that they are compared with the spectra of the others. The OH stretching vibration of bare phenol appears at 3657 cm^{-1}, while that of phenol−N_2 is found at 3652 cm^{-1}, showing the low-frequency shift of 5 cm^{-1}. This small but definitive frequency shift is clear evidence for the hydrogen-bonded structure of phenol−N_2, which has been proposed by Müller-Dethlefs and co-workers.[6,8−10] An alternative structure for phenol−N_2 is an on-top structure, in which van der Waals interactions attract N_2 onto the phenyl ring. In the case of this structure, the OH stretching vibration is expected to show no shift, as is seen in the case of phenol−Ar.[14]

The OH stretching vibration of phenol−CO is found at 3624 cm^{-1}. A weak band is seen at +73 cm^{-1} from the OH stretch band, and it is attributed to a combination band of the OH stretching and an intermolecular vibration. The OH stretch of the phenol site shows a low-frequency shift of −33 cm^{-1} upon the cluster formation with CO. The hydrogen-bonded structure for this cluster has also been proposed by Müller-Dethlefs and co-workers on the basis of the electronic spectroscopy and ab initio calculations.[7,8] Similar to phenol−N_2, the OH frequency shift of phenol−CO clearly supports the hydrogen-bonded structure. The −33 cm^{-1} shift is quite smaller than those of typical hydrogen-bonded clusters of phenol (>100 cm^{-1}),[3−5,17,18] and it reflects the extremely weak hydrogen-bond strength in this cluster.

The IR spectrum of phenol−CO_2 also shows two bands at 3631 and 3718 cm^{-1}. The former band is assigned to the OH stretching vibration, showing the low-frequency shift of −26 cm^{-1}, and the latter is assigned to a combination band of the

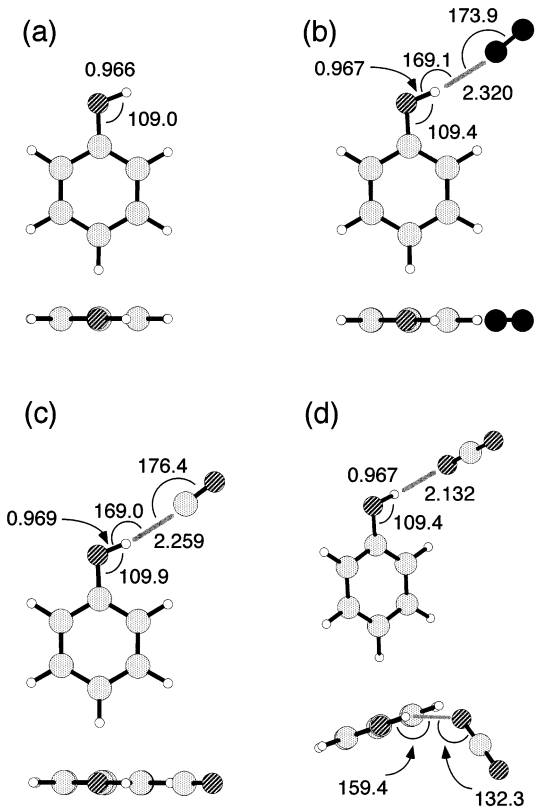

Figure 3. Energy-optimized structures and key geometrical parameters of (a) bare phenol, (b) phenol−N_2, (c) phenol−CO, and (d) phenol−CO_2 in S_0. The calculation level is B3LYP/6-31G(d,p). Units of bond distances and bond angles are Å and deg, respectively.

OH stretch and an intermolecular vibration, as found for phenol−CO. The low-frequency shift of the OH stretch clearly indicates that the hydroxyl group of phenol is bound to CO_2 with a hydrogen bond. Here, it should be noted that the S_1-S_0 origin band of phenol−CO_2 shows the *high*-frequency shift, as seen in Figure 1. In all of the hydrogen-bonded clusters containing phenol known so far, the S_1-S_0 electronic transition localized on the proton-donating phenol site shows a *low*-frequency shift.[1−5] This high-frequency shift in phenol−CO_2 is quite exceptional, though the reason for it is unclear at present.

The OH bandwidth of phenol−CO_2 is rather broader than those of the other clusters. This broadness might be attributed to the contribution of higher clusters, because those electronic transitions overlap with the origin band of the 1:1 cluster. If the second and following CO_2 molecules solvate the phenyl ring moiety of phenol, the OH frequency shift is dominated only by the first solvating CO_2 molecule, which occupies the interaction region with the hydroxyl group, and higher clusters also show similar OH frequency shifts to that of the 1:1 cluster.

We carried out density functional theoretical (DFT) calculations to support the cluster structures based on the IR spectra. The Gaussian 98 program package was used for the calculations.[19] DFT and ab initio calculations of phenol−N_2 and −CO in S_0 have been performed by Müller-Dethlefs and co-workers at various levels of the theory.[6−10] Our calculations at B3LYP/6-31G(d,p)[20] gave essentially the same structures as that proposed by Müller-Dethlefs et al. The energy-optimized structures of the clusters are illustrated in Figure 3.[21] Both phenol−N_2 and phenol−CO have the in-plane hydrogen-bonded structure, in which the sp lone-pair electrons in the N-end or C-end of the solvent molecules are bound to the hydroxyl group of phenol. Also for phenol−CO_2, a hydrogen-bonded structure was found; the hydroxyl group of phenol is bound to one of the sp^2 lone-pair electrons of CO_2. The CO_2 moiety protrudes into the out-of-plane region of the phenyl ring, reflecting the difference in the spatial distribution of the lone-pair electrons from those of N_2 and CO.

The calculated OH stretching frequencies based on the energy-optimized structures are presented in Figure 2 as bar graphs below the observed spectra. They are also listed in Table 1 with the observed frequencies and the calculated values by Müller-Dethlefs and co-workers.[8] The scaling factor of 0.9566 was applied to our calculated frequencies. This scaling factor was determined to reproduce the observed frequency of bare phenol. The calculations at the B3LYP/6-31G(d,p) level qualitatively reproduce the observed OH frequencies. All of the clusters are predicted to show small OH frequencies due to the hydrogen-bond formation, and the order of the magnitude of the shifts (CO > CO_2 > N_2) is also consistent with the observed results. The extremely small OH shift in phenol−N_2 is especially reproduced well with the B3LYP/6-31G(d,p) calculations, while a high-frequency shift is predicted in the MP2/6-31G(d) level calculations.[8] Though the B3LYP calculations well reproduced the experimental results, the B3LYP functional does not describe the dispersion interactions.[8,22] Because the dispersion interaction is generally expected to play an important role in such weakly bound clusters, it should be noted that the good agreement between the experimental and calculated frequencies is regarded as a result of cancellation of errors.

The magnitude of the low-frequency shifts of the OH stretching vibrations is qualitatively interpreted by some molecular constants of the solvent molecules listed in Table 2. Though CO is isoelectronic with N_2, phenol−CO shows a much larger OH frequency shift than phenol−N_2. Polarizability of CO is quite similar to that of N_2, while CO has a dipole moment, and its quadrupole moment is somewhat larger than that of N_2. The larger electrostatic interactions would be responsible for the stronger hydrogen bond in phenol−CO. The OH frequency shift in phenol−CO_2 is slightly smaller than that of phenol−CO but is much larger than that of phenol−N_2. CO_2 has no dipole moment, but its quadrupole moment and polarizability are much larger than those of N_2 and CO. The lack of the dipole−dipole interaction in phenol−CO_2 is compensated with the interactions with the larger quadrupole moment and inductive forces, resulting in the similar OH frequency shift to phenol−CO.

The intermolecular binding energies of phenol−N_2 and −CO in S_0 have been experimentally estimated to be only 435 ± 20 and 659 ± 20 cm^{-1}, respectively.[6,7] These values are close to a typical van der Waals bond energy ($\lesssim$300 cm^{-1}) between an aromatic molecule and an Ar atom.[12] In the case of phenol−Ar in S_0, only the on-top van der Waals cluster is experimentally confirmed so far,[10,14] though a stable minimum of the hydrogen-bonded type has been predicted in theoretical calculations.[5,26] The polarizability and ionization potential of Ar is comparable to those of N_2, CO, and CO_2, as seen in Table 2, suggesting that a similar magnitude of inductive forces and charge transfer can be expected for Ar as a proton acceptor. Therefore, the absence of the hydrogen-bonded structure in phenol−Ar indicates the dominance of the electrostatic interactions in the weak hydrogen bonds in phenol−N_2, −CO, and −CO_2. Of course, it should be noted again that such discussion based on molecular constants for bare molecules is quite qualitative. Decomposition of the interaction energy based on quantum chemical calculations is required for more rigorous discussion.[27]

TABLE 1: Observed and Calculated OH Stretching Vibrational Frequencies of Bare Phenol and Phenol−X (X = N_2, CO, and CO_2) Clusters in cm^{-1}[a]

	S_0				D_0			
		calcd				calcd		
	obsd	B3LYP/ 6-31G(d,p)[c,d]	MP2/ 6-31G(d)[e,f]	B3LYP/ 6-31G(d)[e,f]	obsd	B3LYP/ 6-31G(d,p)[c,g]	MP2/ 6-31G(d)[e,f]	B3LYP/ 6-31G(d)[e,f]
phenol	3657[b]	3657			3534[b]	3534		
phenol-N_2	3652[b] (−5)	3652 (−5)	(+15)		3375 ± 5[b] (−159 ± 5)	3356 (−178)	(−88)	(−150)
phenol-CO	3624[c] (−33)	3606 (−51)	(−8)	(−34)	3323 ± 5[c] (−211 ± 5)	3137 (−397)	(−219)	(−360)
phenol-CO_2	3631[c] (−26)	3647 (−10)			3337 ± 10[c] (−197 ± 10)	3317 (−217)		

[a] Values in the parentheses are shifts from the frequency of the bare molecule. [b] Reference 14. [c] This work. [d] A scaling factor of 0.9566 is applied. [e] Without a scaling factor. [f] Reference 8. [g] A scaling factor of 0.9492 is applied.

TABLE 2: Comparison of Molecular Constants of N_2, CO, CO_2, and Ar

	proton affinity (kcal/mol)	dipole moment[b] (D)	quadrupole moment[c] (10^{-26} esu cm^2)	polarizability[b] (10^{-24} cm^3)	ionization potential[b] (eV)
N_2	118.1		−1.52	1.70	15.58
CO	142.0	0.110	−2.5	1.95	14.01
CO_2	129.2		−4.3	2.91	13.77
Ar	88.2			1.64	15.76

[a] Reference 23. [b] Reference 24. [c] Reference 25.

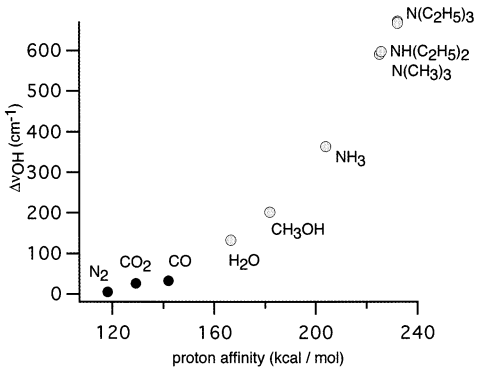

Figure 4. Plot of the shifts of the OH stretching vibrational frequencies versus the proton affinities of the acceptor molecules in phenol−base (1:1) clusters in S_0. The OH frequency shifts in phenol−H_2O, −CH_3-OH, −NH_3, −$NH(C_2H_5)_2$, −$N(CH_3)_3$, and −$N(C_2H_5)_3$ are taken from ref 17.

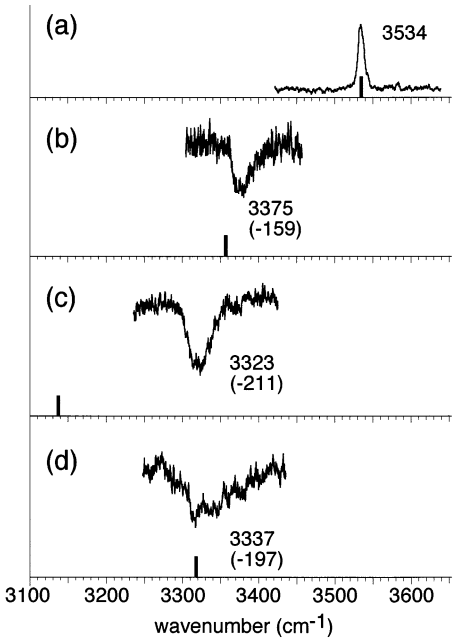

Figure 5. OH stretching vibrational region of IR spectra of (a) bare phenol, (b) phenol−N_2, (c) phenol−CO, and (d) phenol−CO_2 in the cationic ground state (D_0). The infrared photodissociation (IRPD) spectroscopic technique is utilized to measure the spectra. Values in the parentheses are the shifts from the OH vibrational frequency of the bare phenol cation. Bar graphs under the observed spectra show the calculated OH stretching vibrational frequencies based on the energy-optimized structures at the B3LYP/6-31G(d,p) level (see text).

The hydrogen bonds in phenol−N_2, −CO, and −CO_2 are clearly categorized to be the weakest ones ever observed, and it is interesting to examine whether such extraordinary weak hydrogen bonds show the correlation between the OH frequency shifts and the proton affinities of the acceptor molecules, as seen in typical σ-hydrogen-bonded phenol clusters.[17,18] Figure 4 shows a plot of the OH frequency shifts versus proton affinities of acceptor molecules in various phenol−base (1:1) clusters. The frequency shifts of phenol−N_2, −CO, and −CO_2 are so small that their correlation with the proton affinity is not remarkable, when we focus only on these clusters. However, in comparison with the typical σ-hydrogen-bonded phenol clusters, it is clearly seen that these weakly bound clusters well fall on an extrapolation of the correlation curve for the clusters of typical hydrogen-bond strength. This result suggests that the nature of these extremely weak hydrogen bonds is essentially the same as typical σ-hydrogen bonds studied so far.

C. Infrared Spectra in D_0. Figure 5 shows the OH stretching vibrational region of (a) bare phenol cation, (b) $(phenol-N_2)^+$, (c) $(phenol-CO)^+$, and (d) $(phenol-CO_2)^+$ cluster cations. The spectra a and b have been presented in ref 14, and they are reproduced here for comparison with the others. In each spectrum, the cluster cation was produced by REMPI of the corresponding neutral cluster. The IRPD spectroscopic technique was used to measure the spectra of the cluster cations, while the autoionization-detected infrared (ADIR) spectroscopy, which is described in detail in refs 28 and 29, was applied to record the IR spectrum of the bare cation.

The OH stretching vibrational band is found at 3534 cm^{-1} in the bare phenol cation. The OH band of $(phenol-N_2)^+$ appears at 3375 ± 5 cm^{-1}, and the low-frequency shift due to the cluster formation is −159 ± 5 cm^{-1}. The same IR spectrum was also reported by Solcà and Dopfer, who prepared the cluster ion by using a pick-up-type ion source.[15,16] The spectrum of $(phenol-CO)^+$ is similar to that of $(phenol-N_2)^+$, but the low-frequency shift of the OH band becomes more remarkable; the OH band is seen at 3323 ± 5 cm^{-1}, and the low-frequency shift is −211 ± 5 cm^{-1}. The low-frequency shifts of the OH bands are direct evidence for the hydrogen-bonded structure in D_0,

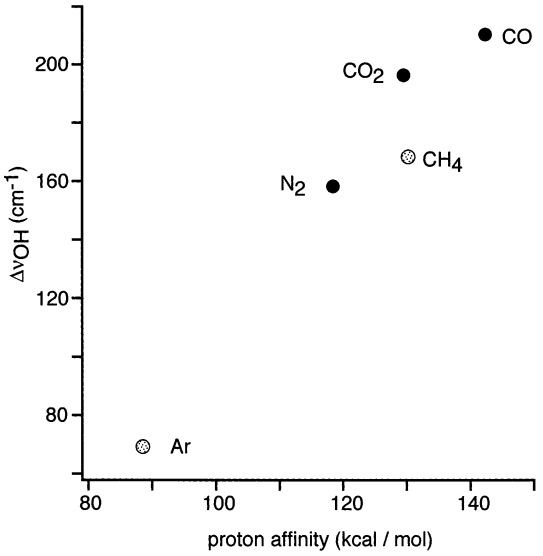

Figure 6. Plot of the shifts of the OH stretching vibrational frequencies versus the proton affinities of the acceptor molecules in the phenol−base (1:1) cluster cations. The OH frequency shifts in $(phenol-Ar)^+$ and $(phenol-CH_4)^+$ are taken from ref 16.

which has first been proposed by Müller-Dethlefs et al.[6−10] The drastic increase of the OH frequency shifts upon ionization reflects the remarkable enhancement of the hydrogen-bond strength, which has been deduced by MATI spectroscopy of the cluster cations.[6,7] The enhancement of the hydrogen-bond strength is clearly attributed to the increase of electrostatic and inductive interactions associated with the positive charge on the phenol site.

The IR spectrum of $(phenol-CO_2)^+$ shows a broad OH stretching band centered at 3337 ± 10 cm^{-1}. The low-frequency shift of -197 ± 10 cm^{-1} indicates that the hydrogen-bonded-structure is held in D_0 and the hydrogen-bond strength is significantly enhanced as seen in the other clusters. The OH bandwidth of $(phenol-CO_2)^+$ is broader than those of the other cluster cations. This is also attributed to the contribution of higher clusters. In IRPD spectroscopy, depletion of the signal intensity of the mass-selected 1:1 cluster cation is measured; therefore, only the 1:1 cluster cation can contribute to the spectrum. However, ionization of neutral higher clusters followed by dissociation in D_0 produces the 1:1 cluster cation having substantial vibrational energy in various bath modes. The OH transition of such a hot cluster cation leads to the broad bandwidth because of the anharmonic coupling between the OH vibration and other bath modes.

The order of the magnitude of the OH frequency shifts (CO > CO_2 > N_2) in the cluster cations is the same as that in the neutrals (i.e., the order of the proton affinities of the acceptors). The plot of the OH frequency shifts in $(phenol-N_2)^+$, $(phenol-CO)^+$, and $(phenol-CO_2)^+$ versus the proton affinities of the acceptors is shown in Figure 6. OH frequencies of the hydrogen-bonded phenol cluster cations with Ar and CH_4 were measured by Solcà and Dopfer.[16] Points for $(phenol-Ar)^+$ and $(phenol-CH_4)^+$ are also added in the plot. A clear correlation between the OH frequency shifts and the proton affinities is seen in the plot, as was partly shown by Solcà and Dopfer.[16] A similar correlation for the NH stretching vibrations in the aniline cluster cations was reported by Nakanaga and co-workers.[30] These results indicate that the proton affinity of the acceptor can be a measure of the hydrogen-bond strength also in cluster cations. In the case of hydrogen-bonded phenol cluster cations, however, experimental determination of OH stretching vibrational frequencies has been limited only for the very weak proton acceptors. OH frequencies in cluster cations with typical proton acceptors, such as water and ammonia, have not been determined because of extremely large frequency shifts.[31−33] It is a future task to probe the correlation in the larger proton affinity region.

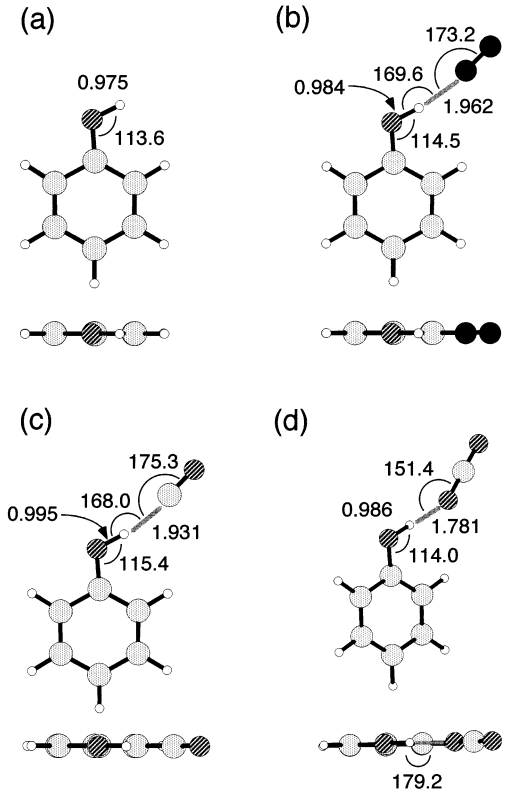

Figure 7. Energy-optimized structures and key geometrical parameters of (a) bare phenol, (b) phenol−N_2, (c) phenol−CO, and (d) phenol−CO_2 in D_0. The calculation level is B3LYP/6-31G(d,p). Units of bond distances and bond angles are Å and deg, respectively.

DFT calculations of energy-optimized structures also support the hydrogen-bonded structure of these cluster cations. The energy-optimized structures at the B3LYP/6-31G(d,p) level are shown in Figure 7. $(Phenol-N_2)^+$ and $(phenol-CO)^+$ have similar in-plane structures to those of the corresponding neutrals; the sp lone-pair electrons in the N- or C-end of the solvent molecule are linearly bound to the hydroxyl hydrogen of the phenol site. The O−H distance of the phenol site, however, becomes much longer, while the intermolecular distance becomes remarkably shorter, reflecting the significant enhancement of the hydrogen-bond strength. These predictions are consistent with the previous theoretical calculations by Müller-Dethlefs et al.[6−10] and Solcà and Dopfer.[15]

On the other hand, the energy-optimized structure of $(phenol-CO_2)^+$ is quite different from that of the neutral cluster. The hydroxyl group of phenol is bound to the sp^2 lone-pair electrons of CO_2, which is in the same plane as the phenyl ring. This is in contrast with the structure of the neutral, in which the CO_2 moiety protrudes into the out-of-plane region of the phenyl ring. No stable minimum similar to the neutral cluster was found for the cationic cluster. In $(phenol-CO_2)^+$, the positive charge is mainly distributed in the phenyl ring because of the much lower ionization potential of phenol (8.51 eV) than that of CO_2 (13.77 eV).[24] Because the carbon atom in CO_2 is positively charged as seen in its negative sign of the quadrupole moment,[25] a large separation between the phenyl ring and the carbon atom of CO_2 stabilizes the cluster when the phenol site is ionized. This might be the reason for the preference of the in-plane structure in D_0.

The calculated harmonic frequencies of the OH stretching vibrations based on the energy-optimized structures of the cluster cations are also listed in Table 1 with those by Müller-Dethlefs and co-workers.[8] The scaling factor of 0.9492 was applied to the results of our B3LYP/6-31G(d,p) calculations. This scaling factor was determined to reproduce the OH frequency of the bare phenol cation. A comparison with the observed spectra is seen in Figure 5; the calculated OH frequencies are shown as bar graphs together with the observed spectra. The calculated OH frequencies qualitatively reproduce the observed spectra; the magnitude of the low-frequency shifts due to the hydrogen-bond formation are much larger than those of the corresponding neutral clusters, reflecting the remarkable enhancement of the hydrogen-bond strength. The order of the magnitude of the shifts ($CO > CO_2 > N_2$), which is the same as that in the neutrals, is also reproduced in the simulation. These good agreements between the observed and simulated spectra support the calculated structures of the cluster cations.

Summary

IR spectroscopy was applied to phenol−CO and $-CO_2$ in a molecular beam to observe the OH stretching vibrations in S_0 and D_0. Both of the clusters show the small but definitive low-frequency shifts of the OH stretching vibration in S_0. These shifts due to the cluster formation are the firm evidence for the hydrogen-bonded structures of these clusters, which have been predicted for phenol−CO on the basis of electronic spectroscopy and ab initio calculations. The magnitude of the OH frequency shifts is quite small, reflecting the very weak hydrogen-bond strength. The OH stretching vibrations in D_0 show much larger low-frequency shifts than those in S_0. This result indicates that the cluster cations hold the hydrogen-bonded structures and the hydrogen-bond strength is remarkably enhanced upon the ionization. Both in S_0 and D_0, the OH frequency shifts correlate well with the proton affinities of the acceptor molecules.

References and Notes

(1) Ito, M. *J. Mol. Struct.* **1988**, *177*, 173.

(2) Mikami, N. *Bull. Chem. Soc. Jpn.* **1995**, *68*, 683.

(3) Ebata, T.; Fujii, A.; Mikami, N. *Int. Rev. Phys. Chem*. **1998**, *17*, 331.

(4) Brutschy, B. *Chem. Rev.* **2000**, *100*, 3891.

(5) Dessent, C. E. H.; Müller-Dethlefs, K. *Chem. Rev.* **2000**, *100*, 3999.

(6) Haines, S. R.; Geppert, W. D.; Chapman, D. M.; Watkins, M. J.; Dessent, C. E. H.; Cockett, M. C. R.; Müller-Dethlefs, K. *J. Chem. Phys*. **1998**, *109*, 9244.

(7) Haines, S. R.; Dessent, C. E. H.; Müller-Dethlefs, K. *J. Chem. Phys.* **1999**, *111*, 1947.

(8) Chapman, D. M.; Müller-Dethlefs, K.; Peel, J. B. *J. Chem. Phys*. **1999**, *111*, 1955.

(9) Watkins, M. J.; Müller-Dethlefs, K.; Cockett, M. C. R. *Phys. Chem. Chem. Phys*. **2000**, *2*, 5528.

(10) Ford, M. S.; Haines, S. R.; Pugliesi, I.; Dessent, C. E. H.; Müller-Dethlefs, K. *J. Electron Spectrosc. Relat. Phenom.* **2000**, *112*, 231.

(11) Weber, Th.; Smith, A. M.; Riedle, E.; Neusser, H. J.; Schlag, E. W. *Chem. Phys. Lett*. **1990**, *175*, 79.

(12) Braun, J. E.; Mehnert, Th.; Neusser, H. J. *Int. J. Mass Spectrom.* **2000**, *203*, 1.

(13) Bürgi, T.; Droz, T.; Leutwyler, S. *Chem. Phys. Lett*. **1995**, *246*, 291.

(14) Fujii, A.; Miyazaki, M.; Ebata, T.; Mikami, N. *J. Chem. Phys*. **1999**, *110*, 11125.

(15) Solcà, N.; Dopfer, O. *Chem. Phys. Lett.* **2000**, *325*, 354.

(16) Solcà, N.; Dopfer, O. *J. Phys. Chem. A* **2001**, *105*, 5637.

(17) Iwasaki, A.; Fujii, A.; Ebata, T.; Mikami, N. *J. Phys. Chem*. **1996**, *100*, 16053.

(18) Fujii, A.; Ebata, T.; Mikami, N. *J. Phys. Chem. A* **2002**, *106*, 8554.

(19) Frisch, M. J.; Trucks, G. W.; Schlegel, H. B.; Scuseria, G. E.; Robb, M. A.; Cheeseman, J. R.; Zakrzewski, V. G.; Montgomery, J. A., Jr.; Stratmann, R. E.; Burant, J. C.; Dapprich, S.; Millam, J. M.; Daniels, A. D.; Kudin, K. N.; Strain, M. C.; Farkas, O.; Tomasi, J.; Barone, V.; Cossi, M.; Cammi, R.; Mennucci, B.; Pomelli, C.; Adamo, C.; Clifford, S.; Ochterski, J.; Petersson, G. A.; Ayala, P. Y.; Cui, Q.; Morokuma, K.; Malick, D. K.; Rabuck, A. D.; Raghavachari, K.; Foresman, J. B.; Cioslowski, J.; Ortiz, J. V.; Stefanov, B. B.; Liu, G.; Liashenko, A.; Piskorz, P.; Komaromi, I.; Gomperts, R.; Martin, R. L.; Fox, D. J.; Keith, T.; Al-Laham, M. A.; Peng, C. Y.; Nanayakkara, A.; Gonzalez, C.; Challacombe, M.; Gill, P. M. W.; Johnson, B. G.; Chen, W.; Wong, M. W.; Andres, J. L.; Head-Gordon, M.; Replogle, E. S.; Pople, J. A. *Gaussian 98*, revision A.7; Gaussian, Inc.: Pittsburgh, PA, 1998.

(20) Stevens, P. J.; Devlin, F. J.; Chablowski, C. F.; Frisch, M. J. *J. Phys. Chem*. **1994**, *98*, 11623.

(21) These calculated structures are visualized by using *MOLCAT*, version 2.5.2: Tsutui, Y.; Wasada, H. *Chem. Lett*. **1995**, 517.

(22) Hobza, P.; Sponer, J.; Reschel, T. *J. Comput. Chem.* **1995**, *16*, 1315.

(23) Hunter, E. L.; Lias, S. G. *J. Phys. Chem. Ref. Data* **1998**, *27*, 413.

(24) *CRC Handbook of Chemistry and Physics*, 76th ed.; Lide, D. R., Ed.; CRC Press: Boca Ration, FL, 1995.

(25) Stogryn, D. E.; Stogryn, A. P. *Mol. Phys.* **1966**, *11*, 371.

(26) Ullrich, S.; Tarczay, G.; Müller-Dethlefs, K. *J. Phys. Chem. A* **2002**, *106*, 1496.

(27) Kitaura, K.; Morokuma, K. *Int. J. Quantum Chem*. **1976**, *10*, 325.

(28) Fujii, A.; Iwasaki, A.; Ebata, T.; Mikami, N. *J. Phys. Chem. A* **1997**, *101*, 5963.

(29) Fujimaki, E.; Fujii, A.; Ebata, T.; Mikami, N. *J. Chem. Phys.* **1999**, *110*, 4238.

(30) Schmid, R. P.; Chowdhury, P. K.; Miyawaki, J.; Ito, F.; Sugawara, K.; Nakanaga, T.; Takeo, H.; Jones, H. *Chem. Phys.* **1997**, *218*, 291.

(31) Sawamura, T.; Fujii, A.; Sato, S.; Ebata, T.; Mikami, N. *J. Phys. Chem.* **1996**, *100*, 8131.

(32) Kleinermanns, K.; Janzen, C.; Spangenberg, D.; Gerhards, M. *J. Phys. Chem. A* **1999**, *103*, 5232.

(33) Gerhards, M.; Jansen, A.; Unterberg, C.; Kleinermanns, K. *Chem. Phys. Lett.* **2001**, *344*, 113.